# Laser Scanner-Based Robotic Coordinate Measuring Machine

Vladimir Gurau *, Andy Gerhardstein, Kalvin Carruthers, and Hank Frazer

Robotics Process Development Laboratory (RPDL),
Department of Manufacturing Engineering, Georgia Southern University, Statesboro, USA
Email: vgurau@georgiasouthern.edu (V.G.); ag09260@georgiasouthern.edu (A.G.);
kc08656@georgiasouthern.edu (K.C.); jf05413@georgiasouthern.edu (H.F.)
*Corresponding author

***Abstract*—The objectives of the research presented in this paper are to design, integrate and demonstrate a robotic Coordinate Measuring Machine (CMM) for digitizing 3D geometries of objects to be used in reverse-engineering applications. The paper describes the mathematical model, the integration of the light detection and ranging (LiDAR) sensor with the automated positioning system and the programming used to attain the technology. The digital reconstruction of an object's 3D model is achieved by applying forward robot kinematics along with homogeneous transforms to the point cloud detected by the LiDAR. The object's geometric features are determined using 2nd-order polynomial best fitted curves of the scanned point clouds using the bisquare fit method. The CMM uses forward robot kinematics along with homogeneous transforms to programmatically compensate for geometric positioning errors resulting from deviations in position and orientation of the CMM components during assembly and from deviations in position and orientation of the workpiece when it is located in its mounting device. The instrument is shown to reconstruct with remarkable qualitative accuracy the 3D model of a turbine blade. Using a better-quality detecting sensor, the instrument can be used as well in automated quality control and inspection applications.**

***Keywords*—Coordinate Measuring Machine (CMM), digitization of 3D models, robotic reconstruction of 3D geometries**

## I. Introduction

Coordinate Measuring Machines (CMMs) are manual or robotic instruments used for the inspection of 3D geometric features of manufactured parts. They generally comprise of four components: the hardware, the probing system, the control system, and the measuring software. The CMM hardware consists of a number or rigid links connected to each other by linear or rotary joints. Typical CMM configurations include the bridge type (gantry), consisting of three mutually perpendicular linear joints in the form of linear positioning slides, or various types of serial-link or parallel-link arms with rotary joints. The total number of joints, linear and rotary defines the Degrees of Freedom (DOF) of the CMM. At the end of the last link is mounted a measuring probe, which can be mechanical, laser, or optical.

The CMM operation involves the movement of the probe relative to the inspected part. The position of the probe may be controlled manually, or each joint may be actuated programmatically by a computer-controlled motor. The CMM joints are equipped with encoders that provide feedback on the values of the angular or linear joint coordinates.

Knowing the joint coordinates and the size of the links, CMMs use forward robot kinematics [1, 2] to determine the coordinates of the points detected by the probe on the surfaces of the inspected part relative to a fixed frame, which can be the world frame (machine home), or a part-referenced frame. This enables the CMM to generate a point cloud representing the digital, or reconstructed model of the object. CMMs further use fitting algorithms based on least squares or best fit methods [3–5] to convert regions of the point cloud to geometric features such as circles, cylinders, planes, etc. This allows CMMs to measure sizes and locations of features, or to determine geometric characteristics of the inspected part such as flatness, circularity, parallelism, straightness, concentricity, runout, etc.

It is evident therefore that a CMM measurement represents a multi-step process where each step contributes to the overall measurement error. Baldwin *et al.* [6] identify sources of CMM measurement errors from factors such as workpiece position and orientation, sensor type and configuration, environment conditions, sampling strategy, fitting algorithms, etc. According to Butler [7], the measuring probe is one of the most important sources of error, accounting for about 60% of errors in a CMM measurement. Ren *et al.* [8] investigated the uncertainties associated with the application of the least squares-based geometric feature characterization method. Other researchers [9–11] investigated geometric positioning errors resulting from the relative position and orientation of the CMM components and from those of the workpiece and proposed various compensation methods. The

Manuscript received July 18, 2023; revised September 2, 2023; accepted October 25, 2023; published February 21, 2024.

influence of temperature on measurements has been investigated among others by Kruth *et al.* [12], Teeuwsen *et al.* [13] and Kim and Chung [14]. A comprehensive review of uncertainties associated with CMM measurements may be found in the work of Mian and Al-Ahmari [15]. The interested reader may find recent research and developments in the field of coordinate measuring machines in references [16–20].

The capital cost of automated CMMs is currently high, ranging roughly between $50,000 for a robotic arm equipped with a mechanical or laser sensor, to $100,000 for a CMM based on machine vision. In this paper, we describe the in-house development of an inexpensive automated CMM (under $3,000). We present the hardware integration, the mathematical model, the programming, and the strategy used by this CMM to programmatically compensate for geometric positioning errors. To the best of our knowledge, there have not been previously published papers detailing the design and integration of automated CMMs. This paper presents the design, integration, and demonstration of a robotic CMM that uses a Light Detection and Ranging (LiDAR) sensor to detect points on the surfaces of the inspected part and generate its digital model.

The rest of the paper is organized as follows: Section II.A describes the integration of the CMM hardware components. Section II.B presents the mathematical model of the robot kinematics specific to the current CMM configuration. This section also describes the mathematical model used to programmatically compensate for geometric positioning errors resulting from deviations in position and orientation of the CMM components during assembly and from deviations in position and orientation of the workpiece when it is located in its mounting device. Section II. C presents the software used for data acquisition and the software used to programmatically control the relative motion between the part to be inspected and the sensor. Section III presents the sensitivity analysis results of two fitting algorithms used to convert regions of the point cloud to geometric features. This section also presents the strategy and the results of compensating for geometric positioning errors resulting from deviations in position and orientation of the CMM components during assembly and from deviations in position and orientation of the workpiece when it is located in its mounting device, as well as the results obtained from digitization of the inspected part. Section IV summarizes the conclusions of this work.

## II. Materials and Methods

### A. System Integration

The integrated CMM (Fig. 1) consists of an automated positioning system with two DOF on which the object to be inspected is mounted, a fixed laser scanner sensor that adds two more DOF to the system and used to detect points on the object's surfaces, a microprocessor, and a computer with *LabView* software.

The two-DOF automated positioning system consists of a rotary joint mounted on top of a linear joint, both joints having parallel axes. The linear joint consists of a 6-inch-travel linear positioning slide (Parker Hannifin) driven by a 5 mm-pitch ball screw that eliminates backlash. The rotary joint consists of an in-house fabricated mounting device for locating the objects to be digitized and mounted on the shaft of a stepper motor. Both linear and rotary joints are actuated by *STP-MTRH-23079* stepper motors (*Automation Direct*), each equipped with an *AMT112Q-V* differential, quadrature encoder (*CUI Devices*) with 1600 pulses per revolution (ppr) that provide closed loop feedback for the positioning system. The stepper motors are controlled by *STP-DRV-6575* stepper motor drivers (*Automation Direct*). The encoders' resolution of 1600 ppr and the 5 mm pitch of the ball screw allow a positional accuracy of the object to be inspected relative to the sensor of 0.225° for the rotary joint and 0.003 mm for the linear joint. The encoders are connected to the microcontroller with RJ45 connectors, each through a *C46* differential-to-single-ended driver (*CNC4PC*). The step, direction and enable terminals of the stepper motor drivers are connected directly to the microcontroller's Digital Outputs (DOs). The *Atmel ATmega2560*—based microcontroller serves mainly as Data Acquisition (DAQ) interface between encoders, motor drivers and the main computer and has two functions: (i) receives positional data from the encoders (number of pulses) and sends it to the computer for processing, and (ii) sends step, direction and enable signals to the stepper motor drivers to jog the rotary and linear axes of the CMM based on commands received from the computer (see Section II.C).

The sensor integrated in the current system is a *RPLiDAR A2* laser scanner (*SLAMTEC*) for which a *LabView* driver was created in-house and integrated in the main software.

The laser scanner, the automated positioning system and the microcontroller are assembled on a C-shape frame made of aluminum extrusion profiles (*80/20*). The fixed lidar is positioned 206 mm above the axis of the rotary joint.

The laser scanner and the microcontroller communicate through serial ports with the main computer on which *LabView* software with *Robotics Module* is installed (see Section II.C).

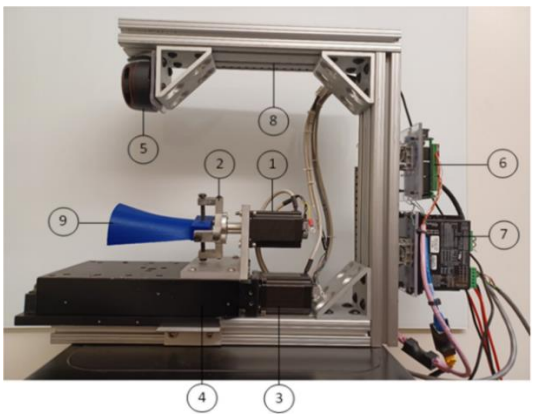


Fig. 1. Coordinate Measuring Machine. 1. stepper motor of the rotary joint; 2. mounting device; 3. stepper motor of the linear joint; 4. linear positioning slide; 5. *RPLiDAR A2* laser scanner; 6. microcontroller; 7. stepper motor drivers; 8. C-shape frame; 9. object to be digitized.

### B. Mathematical Model

The digital reconstruction of an object's 3D geometry is achieved by application of forward robotic kinematics [1, 2] along with homogeneous transforms to the point cloud coordinates detected by the laser scanner on the object surfaces. Fig. 2(a) illustrates the coordinate systems (frames) of the current CMM configuration. The fixed frame *{T1}* is associated to the fixed laser scanner. Frame *{T2}* represents the original position of the scanned object (CMM home position) and is obtained from *{T1}* through a translation along the $x_{T1}$-axis, followed by a rotation of $-\pi/2$ radians about the $y_{T1}$-axis. The moving frame *{T3}* is associated to the moving object that needs to be scanned and is obtained from *{T2}* through a series of linear translations along its $x_{T2}$-axis and/or rotations about its $x_{T2}$-axis. To reconstruct the 3D geometry of the object, the coordinates of its surface points which are detected by the laser scanner, and which are relative to frame *{T1}* must be converted relative to frame *{T3}*. Knowing the coordinates of the points relative to *{T1}*, the coordinates of the points relative to *{T3}* can be calculated as:

$$\begin{pmatrix} x_{T3} \\ y_{T3} \\ z_{T3} \\ 1 \end{pmatrix} = \begin{pmatrix} R & t \\ 0_{1\times 3} & 1 \end{pmatrix}^{-1} \begin{pmatrix} x_{T1} \\ y_{T1} \\ z_{T1} \\ 1 \end{pmatrix} \quad (1)$$

where $R$ represents the resulting orthonormal rotation matrix, $t$ is the 3-component vertical vector $\begin{pmatrix} x \\ y \\ z \end{pmatrix}$ representing the coordinates of the origin of *{T3}* relative to *{T1}* and $0_{1\times 3}$ is the 3-component horizontal vector $(0 \quad 0 \quad 0)$.

In Eq. (1), the matrix

$${}^{\{T1\}}_{\{T3\}}H = \begin{pmatrix} R & t \\ 0_{1\times 3} & 1 \end{pmatrix} \quad (2)$$

represents the homogeneous transform that describes the pose of frame *{T3}* relative to *{T1}* and is calculated as:

$${}^{\{T1\}}_{\{T3\}}H = {}^{\{T1\}}_{\{T2\}}H \times {}^{\{T2\}}_{\{T3\}}H \quad (3)$$

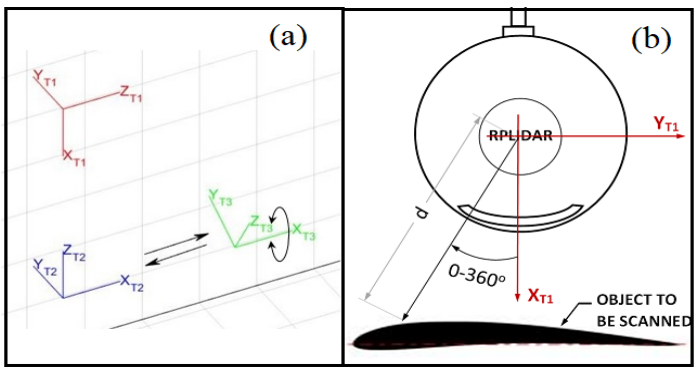


Fig. 2. (a) the coordinate frames associated to the fixed laser scanner *{T1}* (red), to the CMM home position *{T2}* (blue) and to the moving object *{T3}* (green); (b) the polar and cartesian co-ordinate systems of scanned data.

For the current CMM configuration, the homogeneous transform matrix ${}^{\{T1\}}_{\{T2\}}H$ describing the pose of *{T2}* relative to *{T1}* is constant and is determined by the relative positions of the CMM components in the assembly. It is described by a translation of *206* mm along the $x_{T1}$-axis followed by a rotation of $-\pi/2$ radians about the $y_{T1}$-axis (see Section II. A):

$${}^{\{T1\}}_{\{T2\}}H = \begin{pmatrix} \cos(-\pi/2) & 0 & \sin(-\pi/2) & 206 \\ 0 & 1 & 0 & 0 \\ -\sin(-\pi/2) & 0 & \cos(-\pi/2) & 0 \\ 0 & 0 & 0 & 1 \end{pmatrix} \quad (4)$$

The homogeneous transform matrix ${}^{\{T2\}}_{\{T3\}}H$ describing the pose of *{T3}* relative to *{T2}* is variable and is defined by pre-preprogrammed translations of $L$ mm along the $x_{T2}$-axis and/or pre-preprogrammed rotations of $\theta$ radians about the $x_{T2}$-axis:

$${}^{\{T2\}}_{\{T3\}}H = \begin{pmatrix} 1 & 0 & 0 & L \\ 0 & \cos\theta & -\sin\theta & 0 \\ 0 & \sin\theta & \cos\theta & 0 \\ 0 & 0 & 0 & 1 \end{pmatrix} \quad (5)$$

When the object to be reconstructed is located in its mounting device (Fig. 1), there may be linear $y$, $z$ and angular $\theta_y$, $\theta_z$ deviations relative to axis $x_{T2}$. To determine these deviations, the instrument is tested prior to its reconstruction (see Section III), then the following compensating homogeneous transforms are applied along with Eqs. (1)–(5) during the object reconstruction for deviations along and/or about the y-axis, and for deviations along and/or about the z-axis respectively.

$${}^{\{T2\}}_{y}H = \begin{pmatrix} \cos(-\theta_y) & 0 & \sin(-\theta_y) & 0 \\ 0 & 1 & 0 & -y \\ -\sin(-\theta_y) & 0 & \cos(-\theta_y) & 0 \\ 0 & 0 & 0 & 1 \end{pmatrix} \quad (6)$$

$${}^{\{T2\}}_{z}H = \begin{pmatrix} \cos(-\theta_z) & -\sin(-\theta_z) & 0 & 0 \\ \sin(-\theta_z) & \cos(-\theta_z) & 0 & 0 \\ 0 & 0 & 1 & -z \\ 0 & 0 & 0 & 1 \end{pmatrix} \quad (7)$$

In this case, Eq. (3) that describes the pose of frame *{T3}* relative to *{T1}* becomes:

$${}^{\{T1\}}_{\{T3\}}H = {}^{\{T1\}}_{\{T2\}}H \times {}^{\{T2\}}_{y}H \times {}^{\{T2\}}_{z}H \times {}^{\{T2\}}_{\{T3\}}H \quad (8)$$

### C. Software

The CMM shares its programmable functions between an *Atmel ATmega2560*—based microcontroller board and a computer with *LabView* software and *Robotics Module*.

The microcontroller serves mainly as DAQ interface between encoders, motor controllers and the computer and has two functions: (i) Receives positional data from the encoders (number of pulses) and sends it to the computer for processing, and (ii) Sends step and direction signals to the stepper motor drivers to jog the rotary and linear axes of the CMM based on commands received from the computer. The microcontroller C++ source code, *Encoders_and_Motors* which is shared as supplemental material [21] uses two open-source libraries: *TimerThree* [22] to control signal frequencies and *Encoder* [23] to count pulses from the quadrature encoder signals.

The *LabView* project *CMM.lvproj* with its library of subroutines residing on the main computer is shared as supplemental material [24]. The main program, *CMM.vi* was developed in state-machine architecture and has the following functions: (i) Communicates with the *RPLiDAR A2* laser scanner using an in-house developed *LabView* driver; (ii) Selects for analysis only the points on the object whose 3D model must be reconstructed; (iii) Calculates the 2nd-order polynomial best fit curve for the detected points based on the bisquare fit method; (iv) Receives the number of pulses from the encoders and calculates the linear and angular position of the object to be reconstructed relative to frame *{T2}*; (v) Sends step and direction commands to the stepper motor drivers to jog the linear and the rotary axes to the desired positions; (vi) Converts the coordinates of the detected points from frame *{T1}* to frame *{T3}* using Eqs. (1)–(5) and (8); (vii) applies the homogeneous transforms (6) and/or (7) to compensate for the deviations in position and orientation of the object relative to axis $x_{T2}$; (viii) Serves as Graphical User Interface (GUI) for the operator to select the sequence of rotations and translations necessary to automatically expose the object to be reconstructed to the laser scanner.

To enable communication between the *RPLiDAR A2* laser scanner and the host computer, a *LabView* driver was created and integrated with the *LabView* program. The driver which is shared as supplemental material [25] is used by the host computer to send and receive binary data request/response packets to and from the laser scanner based on the *SLAMTEC* protocol [26]. The host computer sends request packets to reset, scan or stop the scanner, or request information regarding the sensor's "health" status. The 30 bits long data response fields are parsed and regrouped according to the communication protocol [26] into data representing the signal quality, the angle, and the distance to reflected points.

The *RPLiDAR A2* scanner detects objects situated at 360° around it. To select only the points on the object that need to be reconstructed, the program removes the outliers outside the (−50 mm, 40 mm) interval on $y_{T1}$-axis and outside the (170 mm, 230 mm) interval on $x_{T1}$-axis (see Fig. 2b). Only the points characterized by a signal quality above 15 are retained. At each relative position between the object and the scanner, the program fetches scanned data until at least 100 points along the profile to be reconstructed are accumulated.

The features of the object to be reconstructed are defined by 2nd-order polynomial best fit curves of the scanned points using the bisquare fit method (see Section III).

The CMM positions the object to be reconstructed relative to the laser scanner by sending step and direction signals to the stepper motor drivers and by using closed loop feedback from the encoders. The operator uses the *LabView* GUI to pre-select a sequence of $L$ mm translations along the $x_{T2}$-axis and of $\theta$ radians rotations about the same axis to position the object. The program calculates the number of pulses to be counted by encoders for the rotary and for the translation motion respectively, as shown in Eqs. (9) and (10).

$$n_{rot} = 1600 \times \theta / 2\pi \tag{9}$$

$$n_{transl} = 1600 \times L/5 \tag{10}$$

The program then sends step and direction signals to the stepper motor controllers until the encoders finish counting the number of pulses Eqs. (9) or (10).

Prior to the object reconstruction process, the operator uses the *LabView* GUI to determine the linear *y*, *z* and the angular $\theta_y$, $\theta_z$ deviations of the object alignment relative to axis $x_{T2}$ (see Section III). If such misalignments exist, the program compensates for them using Eqs. (6) and/or (7).

At each relative position between the object and scanner, the program determines the curve on the object surface by applying the homogeneous transforms Eqs. (1)–(8) to the best fit curve of the 100 points scanned by the laser scanner. The process repeats for each relative position between object and scanner until the desired 3D geometry is digitized.

## III. Results and Discussion

The capability of the CMM to digitize 3D geometries was tested on the 3D printed model of a turbine blade. At each scanned station, the blade's upper and lower cambers were digitized by fitting an n-order polynomial best fit curve of the scanned points. Fig. 3 shows the original point clouds (green dots) detected for (a) the upper camber, and (b) the lower camber of the airfoil sections and their best fit curves (continuous lines) obtained using (1) a 2nd-order polynomial, (2) a 3rd-order polynomial, and (3) a 4th-order polynomial. Point clouds generated by a LiDAR are known to contain points scattered by the edges of the scanned objects. These scattered points become outliers that alter the shape of the fit curve. Fig. 3 shows the scattered points at the leading and trailing edges of the airfoil cambers and their effect on the best fit curves. Two fitting methods were tested: the least square and the bisquare fit method. Out of the two fitting methods, the bisquare fit method iteratively eliminates the outliers and has been determined therefore to be more robust for the current application.

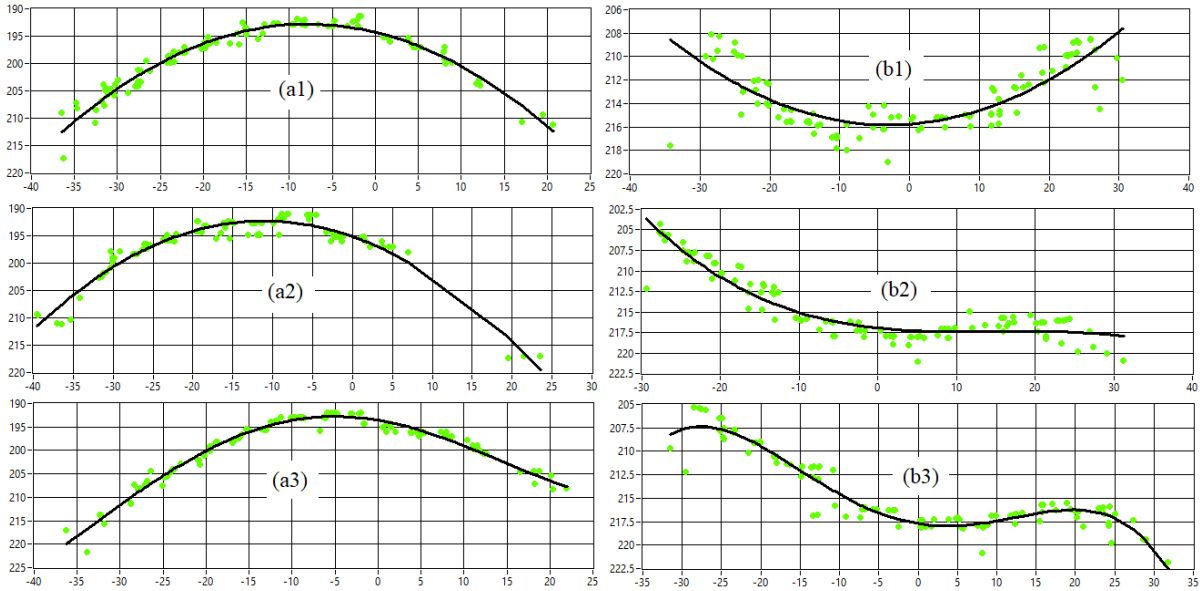


Fig. 3. The effect of the scattered points (outliers) at the leading and trailing edges of the airfoil cambers and the effect of the polynomial order -*n* on the best fit curves. Original point clouds (green dots) detected for (a) the upper camber, and (b) the lower camber of the airfoil sections and their best fit curves (continuous lines) obtained using (1) a 2nd-order polynomial, (2) a 3rd-order polynomial, and (3) a 4th-order polynomial.

A sensitivity test was further carried out to determine the polynomial order–n that best fits the point clouds for the upper and lower cambers of the airfoil sections. Fig. 3 shows that polynomials of order higher than 2 generate curves with inflection points that are atypical to the tested airfoil profiles. The 2nd-order polynomial best fit curve based on the bisquare fit method was selected for fitting the point clouds.

As mentioned in Section I, a major source of CMM measurement errors is related to geometric positioning errors resulting from deviations in position and orientation of the CMM components during its assembly and from deviations in position and orientation of the workpiece when the latter is located in its mounting device. For the current CMM configuration, these errors translate to linear $y$, $z$ and angular $\theta_y$, $\theta_z$ deviations of the axis of the object to be scanned relative to axis $x_{T2}$.

Fig. 4 shows the digitized upper and lower cambers (a) in a calibrated instrument, (b) in an instrument with linear $y$ and $z$ deviations, (c) in an instrument with angular $\theta_z$ deviation and (d) in an instrument with angular $\theta_y$ deviation. When such deviations exist, the instrument applies programmatically the compensating homogeneous transforms Eqs. (6) and (7) along with Eqs. (1)–(5) during the object reconstruction. To determine the deviations, the instrument was tested by comparing the relative positions of the digitized upper and lower cambers of an airfoil section. While autotuning algorithms can be implemented for this purpose, in this work the instrument was calibrated by trial-and error, by adjusting the $y$, $z$, $\theta_y$ and $\theta_z$ parameters in Eqs. (6) and (7) until all deviations between the digitized upper and lower cambers of an airfoil section were eliminated (Fig. 4(a)).

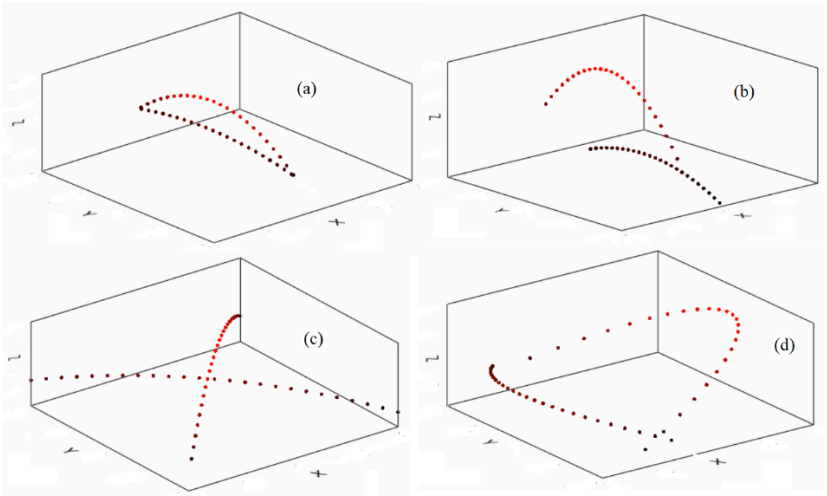


Fig. 4. Reconstructed upper and the lower cambers (a) in a calibrated instrument, (b) in an instrument with linear *y* and *z* deviations, (c) in an instrument with angular $\theta_z$ deviation, and (d) in an instrument with angular $\theta_y$ deviation.

In the current application, the instrument was calibrated with the offset values shown in Table I.

TABLE I. OFFSET VALUES IN THE HOMOGENEOUS TRANSFORMS (6) AND (7) USED TO COMPENSATE THE GEOMETRIC ERRORS IN THE CURRENT INSTRUMENT SETUP

| Parameter | Value | Units | Eq. |
|---|---|---|---|
| $y$ | −4.0 | mm | (6) |
| $z$ | −3.7 | mm | (7) |
| $\theta_y$ | 0 | deg | (6) |
| $\theta_z$ | 0 | deg | (7) |

A segment of the turbine blade was digitized by scanning 30×1 mm apart sections of its suction and pressure surfaces. Each upper and lower cambers were defined by 25 equally spaced points. Fig. 5 shows the isometric views, the front views (along the x-axis) and the side views (along the y-axis) of the digitized suction and pressure surfaces. A limitation of this study is that no datum features were defined for the digitized 3D model to reference the sizes and locations of the airfoil cambers and enable their comparison to the scanned object. While no quantitative measurements were taken to compare the sizes of the blade's geometric features to those of the digitized 3D model, Fig. 5 shows that the instrument could reconstruct the 3D geometry of the turbine blade with remarkable qualitative accuracy.

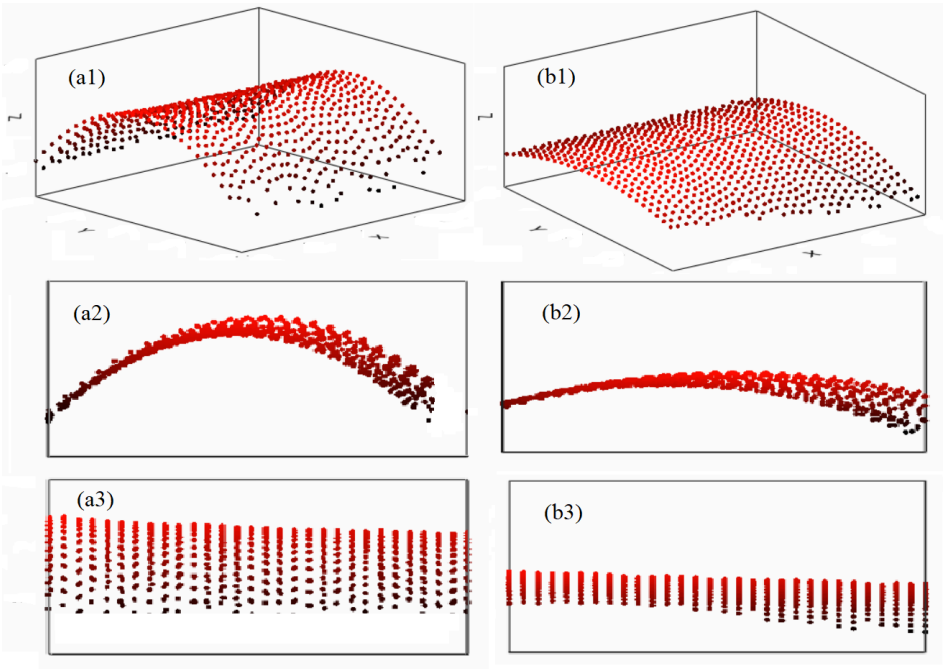


Fig. 5. Reconstructed section of turbine blade; (a) suction surface; (b) pressure surface; (1) isometric view, (2) front view (along the x-axis), and (3) side view (along the y-axis).

A second limitation of this work is that the *RPLiDAR A2* laser scanner used is not conceived as a CMM probe. Using a better-quality detecting sensor, the instrument can be used as well in automated quality control and inspection applications.

The file containing the 3D coordinates of the points representing the digitized model is shared as supplemental material [27].

## IV. CONCLUSIONS

A robotic coordinate measuring machine for digitizing 3D geometry of objects was designed, integrated, and demonstrated for use in reverse-engineering applications.

The capability of the CMM to digitize 3D geometries was tested on a 3D printed model of a turbine blade. The digital reconstruction of the blade's 3D model was achieved by application of forward robotic kinematics along with homogeneous transforms to the point cloud detected by the LiDAR.

The blade's geometric features were determined using *n*-order polynomial best fitted curves of the scanned point clouds. Sensitivity tests were carried out to determine the polynomial order – *n* that best fits the point clouds for the upper and lower cambers of airfoil sections. It was determined that polynomials of order higher than 2 generate curves with inflection points that are atypical to the tested airfoil profile. The 2$^{nd}$-order polynomial best fit curve based on the bisquare fit method was further employed for fitting the point clouds.

To compensate for geometric positioning errors resulting from deviations in position and orientation of the CMM components during assembly and from deviations in position and orientation of the workpiece when it is located in its mounting device, the instrument was tested by comparing the relative positions of the digitized upper and lower cambers of an airfoil section. To compensate for these errors, the instrument applies homogeneous transforms during the object reconstruction.

A segment of the turbine blade was digitized by scanning 30 sections of its suction and pressure surfaces. While no quantitative measurements were taken to compare the sizes of the blade's geometric features to those of the digitized 3D model, the results indicate that the instrument could reconstruct the 3D geometry of the turbine blade with remarkable qualitative accuracy. Using a better-quality detecting sensor, the instrument can be used as well in automated quality control and inspection applications.

## Conflict of Interest

The authors declare no conflict of interest.

## Author Contributions

Conceptualization, V.G.; methodology, V.G.; software, V.G. and A.G..; validation, V.G., A.G., K.C. and H.F.; investigation, V.G., A.G., K.C. and H.F.; writing - original draft preparation, V.G.; writing - review and editing, A.G.; supervision, V.G.; project administration, V.G. All authors have read and agreed to the published version of the manuscript.

## References


[1] P. Corke, "Forward kinematics," *Robotics, Vision and Control. Fundamental Algorithms in MATLAB*, 2nd ed. B. Siciliano, O. Khatib, Eds. Berlin: Springer, 2011, ch. 7.1 pp. 193–204.

[2] J. Craig, "Manipulator kinematics," *Introduction to Robotics Mechanics and Control*, 4th ed. NY: Pearson, 2018, ch. 3, pp. 67–108.

[3] G. A. Watson, "Least squares fitting of circles and ellipses to measured data," *BIT Numerical Mathematics*, vol. 39, pp. 176–191, 1999.

[4] K. Kanatani and P. Rangarajan, "Hyper least squares fitting of circles and ellipses," *Computational Statistics and Data Analysis*, vol. 55, pp. 2197–2208, 2011.

[5] F. Liu, G. Xu, L. Liang, Q. Zhang, and D. Liu, "Least squares evaluations for form and profile errors of ellipse using coordinate data," *Chinese Journal of Mechanical Engineering*, vol. 29, pp. 1020-1028, 2016.

[6] J. M. Baldwin, K. D. Summerhays, D. A. Campbell, and R. P. Henke, "Application of simulation software to coordinate measurement uncertainty evaluations," *Measure*, vol. 2, pp. 40–52, 2007.

[7] C. Butler, "An investigation into the performance of probes on coordinate measuring machines," *Ind. Metrol*., vol. 2, pp. 59–70, 1991.

[8] M. J. Ren, C. F. Cheung, and L. B. Kong, "A task specific uncertainty analysis method for least-squares-based form characterization of ultra-precision freeform surfaces," *Meas. Sci. Technol*., vol. 23, 054005, 2012.

[9] G. Zhang, R. Veale, T. Charlton, B. Borchardt, and R. Hocken, "Error compensation of coordinate measuring machines," *CIRP Ann. Manuf. Technol*., vol. 34, pp. 445–448, 1985.

[10] P. S. Huang and J. Ni, "On-line error compensation of coordinate measuring machines," *Int. J. Machine Tools Manuf*., vol. 35, pp. 725–738, 1995.

[11] G. Hermann, "Volumetric error correction in coordinate measurement," in *Proc. 4th Serbian-Hungarian Joint Symposium on Intelligent Systems*, Subotica, Serbia, 2006, pp. 409–416.

[12] J. P. Kruth, P. C. Vanherck, and C. Van den Bergh, "Compensation of static and transient thermal errors on CMMs," *CIRP Ann. Manuf. Technol*., vol. 50, pp. 377–380, 2001.

[13] J. W. M. C. Teeuwsen, J. A. Soons, and P. H. J. Schellekens, "A general method for error description of CMMs using polynomial fitting procedures," *CIRP Ann. Manuf. Technol*., vol. 38, pp. 505–510, 1989.

[14] K. D. Kim and S. C. Chung, "Accuracy improvement of the on-machine inspection system by correction of geometric and transient thermal errors," *Trans. NAMRI/SME*, vol. 31, pp. 209–216, 2003.

[15] S. H. Mian and A. Al-Ahmari, "New developments in coordinate measuring machines for manufacturing industries," *Int. J. Metrol. Qual. Eng*., vol. 5, pp. 1–10, 2014.

[16] Y. Sun, L. Lu, F. Wu, S. Xiao, J. Sha, and L. Zhang, "Error analysis of a coordinate measuring machine with a 6-DOF industrial robot holding the probe," *Actuators*, vol. 12, pp. 1–14, 2023.

[17] F. Mohammadi, M. Mirhashemi, and R. Rashidzadeh, "A coordinate measuring machine with error compensation in feature measurement: Model development and experimental verification," *Int. J. Adv. Manuf. Technol.*, 2022.

[18] W. Zaborowski, W. Harmatys, and A. Gąska, "The importance of differences in results obtained from measurements with various measuring systems and measuring modes in industrial practice," *Appl. Sci*., vol. 12, 12412, 2022.

[19] S. M. Stojadinovic, V. D. Majstorovic, A. Gąska, J. Sładek, and N. M. Durakbasa, "Development of a coordinate measuring machine-based inspection planning system for Industry 4.0," *Appl. Sci*., vol. 11, 8411, 2021.

[20] O. Abdulhameed, A. Al-Ahmari, S. H. Mian, and M. K. Aboudaif, "Path planning and setup orientation for automated dimensional inspection using coordinate measuring machines," *Mathematical Problems in Engineering*, vol. 2020, 2022.

[21] V. Gurau. (April 2023). Encoders and Motors.ino. Supplemental Files: Laser Scanner-Based Robotic Coordinate Measuring Machine. [Online]. Available: https://digitalcommons.georgiasouthern.edu/data/13/

[22] P. Stoffregen. TimerThree Library. *github.com*. [Online]. Available: https://github.com/PaulStoffregen/TimerThree

[23] P. Stoffregen. "Encoder Library", *github.com*, [Online]. Available: https://github.com/PaulStoffregen/Encoder

[24] V. Gurau. (April 2023). CMM LabView Project. Supplemental Files: Laser Scanner-Based Robotic Coordinate Measuring Machine. [Online]. Available: https://digitalcommons.georgiasouthern.edu/data/13/

[25] V. Gurau. (April 2023). LabView driver for RPLiDAR A2 laser scanner. Supplemental Files: Laser Scanner-Based Robotic Coordinate Measuring Machine. [Online]. Available: https://digitalcommons.georgiasouthern.edu/data/13/

[26] SLAMTEC. (February 2022) RPLIDAR. Interface Protocol and Application Notes. [Online]. Available: https://bucket-download.slamtec.com/6494fd238cf5e0d881f56d914c6d1f355c0f582a/LR001_SLAMTEC_rplidar_protocol_v2.4_en.pdf

[27] V. Gurau. (April 2023). Point coordinates of the digitized model. Supplemental Files: Laser Scanner-Based Robotic Coordinate Measuring Machine. [Online]. Available: https://digitalcommons.georgiasouthern.edu/data/13/